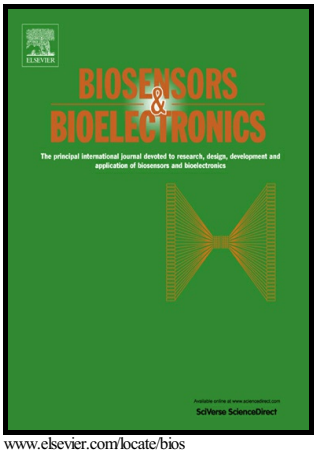

www.elsevier.com/locate/bios

Ultrasensitive microfluidic paper-based electrochemical/visual biosensor based on spherical-like cerium dioxide catalyst for miR-21 detection

Xiaolu Sun, He Wang, Yannan Jian, Feifei Lan, Lina Zhang, Haiyun Liu, Shenguang Ge, Jinghua Yu

PII: S0956-5663(18)30030-7
DOI: https://doi.org/10.1016/j.bios.2018.01.025
Reference: BIOS10218

To appear in: *Biosensors and Bioelectronic*

Received date: 21 October 2017
Revised date: 4 January 2018
Accepted date: 11 January 2018

Cite this article as: Xiaolu Sun, He Wang, Yannan Jian, Feifei Lan, Lina Zhang, Haiyun Liu, Shenguang Ge and Jinghua Yu, Ultrasensitive microfluidic paper-based electrochemical/visual biosensor based on spherical-like cerium dioxide catalyst for miR-21 detection, *Biosensors and Bioelectronic,* https://doi.org/10.1016/j.bios.2018.01.025

Ultrasensitive microfluidic paper-based electrochemical/visual biosensor based on spherical-like cerium dioxide catalyst for miR-21 detection

Xiaolu Sun[a], He Wang[a], Yannan Jian[a], Feifei Lan[a], Lina Zhang[b], Haiyun Liu[a*], Shenguang Ge[a,b*], Jinghua Yu[a]

[a] *Institute for Advanced Interdisciplinary Research, University of Jinan, Jinan 250022,P. R. China.*

[b] *Shandong Provincial Key Laboratory of Preparation and Measurement of Building Materials, University of Jinan, Jinan 250022, P. R. China*

[*]Corresponding author. Tel.: +86-531-82767161; fax: +86-531-82765956. chm_gesg@163.com (S. Ge).

Abstract

In this work, an electrochemical biosensor based on Au nanorods (NRs) modified microfluidic paper-based analytical devices (μPADs) were constructed for sensitive detection of microRNA (miRNA) by using cerium dioxide - Au@glucose oxidase (CeO_2-Au@GOx) as an electrochemical probe for signal amplification. Au NRs were synthesized by in-situ growth method in μPADs surface to enhance the conductivity and modified hairpin probe through Au-S bonds. The construction of "the signal transducer layer" was carried out by GOx catalyzing glucose to produce H_2O_2, which was further electrocatalyzed by CeO_2. After the biosensor was constructed, an obvious electrochemical signal was observed from the reduction of H_2O_2. In order to make the detection more convincing, the visual detection was performed based on the oxidation of 3,3',5,5'-tetramethylbenzidine by H_2O_2 with the help of Exonuclease I. The electrochemical biosensor provided a wide linear range of 1.0 fM to 1000 fM with a relatively low detection limit of 0.434 fM by the electrochemical measurement.

Linear range of 10 fM to 1000 fM with a relatively low detection limit of 7.382 fM was obtained by visual detection. The results indicated the proposed platform has potential utility for detection of miRNA.

Keywords: Cerium dioxide; Electrochemical biosensor; Microfluidic paper-based analytical device; MicroRNA.

1. Introduction

MicroRNA (miRNA) is an important class of small single-stranded noncoding RNA (containing about ~19-23 nucleotides), which can influence many biological processes and regulate the expression of target genes (Hou et al. 2015; Ma et al. 2107). Therefore, sensitive and accurate detection of miRNA plays an important role in better understanding the disease-related biological processes and further validating their function in clinical diagnosis (Liu et al. 2016). So far, a variety of analytical methods have been developed for miRNA detection such as surface plasmon resonance (Fang et al. 2006), bioluminescence assay (Cissell et al. 2008), and microassay analysis (Thomson et al. 2004). However, these methods usually have some limitations, such as poor sensitivity, time-consuming, and complicated instruments (Liu et al. 2015b). In recent years, electrochemical biosensors have attracted much attention due to inherent advantages of simple operation, low-cost, fast response and high sensitivity (liu et al. 2013). However, miRNA in biological samples has the disadvantage of susceptibility to degradation, small size (Torrente-Rodríguez et al. 2016), and the low abundance (Tao et al. 2017). The desire to enhance the detection sensitivity of biosensor for rapid and accurate analyzing miRNA is urgent.

To achieve the high sensitivity of electrochemical biosensor, an important component needs to be improved: “the recognition layer”. Therefore, Au nanorods (NRs) was synthesized in this work, which achieving the improvement of electrode surface conductivity, promoting electron transfer and providing abundant sites for capture biomolecules. Besides, “the signal transducer layer” was the other key component that needed to be improved for enhancing the biosensor sensitivity. Cerium dioxide (CeO_2) have widespread applications in biosensor owing to its

outstanding catalytic performance (Li et al. 2017), anti-inflammatory (Jampaiah et al. 2016), superior biocompatibility and high adsorption capability (Mitsudome et al. 2015). More importantly, CeO_2 (Liu et al. 2015) could catalyze the reaction of peroxidase substrate 3,3',5,5'-tetramethylbenzidine (TMB) in the presence of H_2O_2 (Jiao et al. 2012). In order to increase the electron transfer effect between materials and electrode surface, Au nanoparticles (NPs) were introduced. Recent study has been proved that Au NPs possess many advantages of good biocompatibility (Ye et al. 2017), favorable physical and chemical attributes (Yan et al. 2015). In order to enhance the quantity of Au NPs in the CeO_2 surface, Au NPs fixed onto CeO_2 surface via DNA hybridize instead of forming CeO_2/Au NPs composites directly. This method is beneficial to reduce influence of the steric hindrance and immobilized more Au NPs. Moreover, glucose oxidase (GOx) fixed onto Au NPs surface because its catalysis will produce H_2O_2. Electrons generated by reduction of H_2O_2 can be delivered quickly to the electrode surface due to excellent electron transfer efficiency of Au NPs. Therefore, the synergetic effect of CeO_2 and Au@GOx improved the catalytic properties, which can further increase the chromogenic reaction efficiency toward the TMB.

In order to develop a rapid, portable, and renewable method for convenient and sensitive detection of biomolecules, microfluidic paper-based analytical devices (μPADs) have been introduced into the biosensor. Paper is a biocompatible porous cellulose fiber web with large surface area and porous nature. The first patterned paper was proposed by whitesides and co-workers (Martinez et al. 2010). To date, μPADs have a fast progress in bioanalytical applications (Martinez et al. 2007; Su et al. 2007).

In this study, we designed an ultrasensitive catalysis amplified electrochemical biosensor for detection of miR-21 based on μPADs. As shown in Scheme 1, CeO_2 labelled DNA S1 hybridized with Au@GOx labelled DNA S2 to form an electrochemical probe (CeO_2-Au@GOx). Au NRs modified μPADs (Au-μPADs) was employed for the immobilization of hairpin probe DNA (HP) by Au-S bond. In the presence of target miRNA, after the HP was hybridized with miRNA to open its

hairpin structure, the retained single-strand fragment of HP further hybridized with electrochemical probe labelled capture DNA (capDNA). In order to achieve electron transport for enhancing electrochemical signals, a mass of $Ru(NH_3)_6^{3+}$ as electron mediator was intercalated into DNA duplex to form an electron bridge through electrostatic adsorption (Cheng et al. 2015; Mahmoud et al. 2017). It is worth noting that the proposed biosensor provides an interesting method for semi-quantitative detection by chromogenic reaction and quantitative detection via electrochemical technology. In order to achieve semi-quantitative detection on μPADs, Exonuclease I (Exo I) was introduced in biosensor. As we know, Exo I with digestion function can stimulate the nucleotides of single-stranded DNA to move in the direction of 3′ to 5′, and it has been successfully implemented to digest the aptamer (Zhang et al. 2016). In addition, GOx loaded on Au NPs effectively catalyzed the oxidation of glucose to gluconic acid, accompanied with the generation of H_2O_2. Then, a color change of TMB can be read out directly in catalysis process of CeO_2 towards the reduction of H_2O_2, leading to fast detection for miR-21. As a result, the deeper color and the increasing electrochemical signal would be obtained with the increasing of miR-21. The good performance showed its general and promising way for the detection of miRNA in clinical applications.

2. Experimental

2.1. Design of the μPADs

The μPADs were designed for miRNA detection (details in the supplementary information) according to previous reported work with modification (Yang et al. 2017) as shown in Scheme 2. The paper-based device was comprised of channel tab, detection tab and reference tab with the same size (30 mm × 30 mm). The channel tab and detection tab were used for colorimetric detection, and detection tab and reference tab were applied for electrochemical detection. On the channel tab, the circle that coincides with the size of detection tab were perforated and the rectangular channels (3.5 mm length × 2 mm width) were hydrophilic zones for connecting sample and

pretreated solution. On the detection tab, the hydrophilic circle in center with the diameter of 6 mm is sampling zone “a” and the two circles closest to central circle with the diameter of 4 mm is colorimetric zone “b”. The other four circles with the same diameter as are pretreatment zone “c, d”. Furthermore, a working electrode was printed on one side of the zone a, counter electrode and reference electrode were printed on white hydrophilic area of reference tab after flipping over μPADs. Therefore, the three-electrode system which fabricated on the μPADs was completed. After folding along with line 2, the three electrodes were connected by the filling solution for electrochemical detection of miRNA. Then, after folding along with line 1, the semi-quantitative detection by chromogenic reaction was carried out with the channel connecting the sample zone, pretreatment zone and the detection zone.

2.2. Preparation of Au-μPADs

In order to enhance the electrochemical signal and enlarge effective electrode surface area for sensitive detection of miRNA, the Au-μPADs was obtained through growth of Au nanorods layer on the surfaces of cellulose fibers based on in-situ growth mechanism according to our previous works with slight modifications (Ge et al. 2017). And a detailed procedure was described in the supplementary information.

2.3. Preparation of Au NPs

Au NPs were prepared using the procedures reported previously (Shao et al. 2011). And detailed procedures of Au NPs were described in the supplementary information.

2.4. Preparation of spherical-like CeO_2

The spherical-like CeO_2 were synthesized with slightly modification according to the previous work (Wei et al. 2016). The typical synthesis procedure was described in the supplementary information.

2.5. Preparation of CeO_2-Au@GOx

All DNA and miRNA sequences used in the experiment depicted in Table S1. The synthesis procedure was described in the supplementary information.

2.6. Fabrication of the miRNA biosensor

First of all, on the sample zone of the detection tab, 10 μL of thiol-modified HP (2.5 μM) was dropped onto Au-μPADs surface for 16 h at 4℃, resulting in assembling HP on the modified electrode via Au-S affinity. After that, the modified electrode was rinsed with ultrapure water to remove excess HP. The nonspecific binding sites were blocked with 10 μL of hexanethiol (HT) (1.0 mM) for 40 min. Subsequently, 10 μL of mixture containing different concentrations of target miRNA was dripped onto the modified electrode and incubated for 2 h at 4℃. After rinsing with ultrapure water, the modified electrode was incubated with 10 μL of CeO_2-Au@GOx for 2 h at 4℃. $Ru(NH_3)_6^{3+}$ (10 μL, 1 mM) was intercalated into the double-stranded DNA through electrostatic interation and followed by washing with buffer solution for three times. After that, PBS solution (0.1 M, pH 8.0) containing glucose and the different concentration of miRNA were added in the sample zone, the designed μPADs connected to the electrochemical workstation to conduct electrochemical measurement for quantitative detection. Thereafter, 10 U of Exo I was added in the sample zone a and the CeO_2 far away from the surface of the μPADs due to hydrolysis of HP. Then, the identical solution of 6 mM glucose and 0.8 mM TMB was dropped on the pretreatment zone c1, c2 and zone d1, d2 respectively. Finally, along fold line 1, the sample zone and colorimetric zone or pretreatment zone and colorimetric zone would be connected by channel in channel tab to assist sample solution and pretreatment solution flowing into b1 and b2 zone. It is worth mentioning that zone b2 cannot receive the fluid from zone c2 due to the absence of channel leading to the color without any change in absence of glucose, which used for blank control.

3. Results and discussions

3.1. Possible mechanism of the proposed biosensor

The electrochemical probe with peroxidase-like catalytic properties to H_2O_2 was

used for building miRNA biosensor based on Au NRs modified μPADs by combining colorimetric and electrochemical technology, the possible mechanism illustrated in Scheme 1. In the presence of miRNA, the hairpin structure of HP would be opened and the remaining fragments will hybridize with capDNA, which led to the linkage of the electrochemical probe to the surface of biosensor. In addition, $Ru(NH_3)_6^{3+}$ molecules are incorporated into the duplex DNA via electrostatic interaction to accelerate the electron transfer. Herein, a catalysis amplified miRNA biosensor based on the spherical-like CeO_2, GOx, Au NPs and $Ru(NH_3)_6^{3+}$ was successfully fabricated. Following that, the significant reduction current was obtained with the electrochemical reduction of H_2O_2 for conducting electrochemical detection based on three electrodes screen-printed on μPADs. Meanwhile, the introduction of spherical-like CeO_2 will catalyze the oxidation of TMB by H_2O_2, which is produced by the oxidation of glucose in the presence of GOx. TMB lost electron to transform into an oxidation product and the colorless solution turned to blue immediately, indicating the miRNA biosensor was successfully constructed for achieving semi-quantitative detection of miR-21. Therefore, an ultrasensitive detection for miRNA was achieved by combining electrochemical means and colorimetric methods.

3.2. Characterization of Au-μPAD, Au NPs and spherical-like CeO_2

The morphological features of bare paper and Au-μPADs were directly exhibited by different magnification of scanning electron microscope (SEM) images in Figure 1A and Figure 1B、C. The bare paper with large surface area and porous nature consists of many fibers, which can immobilize the Au NRs well. However, in order to address the problem of poor conductivity of paper, Au NRs arrays were obtained to modifiy on cellulose fibers of paper sample zone. As depicted in Figure 1B and Figure 1C, the Au NRs arrays were uniformly and densely grown on the surfaces of the paper electrode due to its strong interaction with the celluloses based on the in situ growth mechanism (Yang et al. 2017). The Au NRs not only enhanced the conductivity of the paper electrode, but also provided a large surface area for the subsequent anchored of HP via the Au-S bond. Upon further magnification, Au NRs with a diameter of ~20

nm could be clearly observed in the Figure 1C, demonstrating the successful preparation of the Au NRs. Besides, the crystal structures of bare paper and Au-μPADs were characterized by X-ray diffraction (XRD) patterns as shown in Figure 1D. In contrast to the XRD pattern of bare paper (curve a), three distinguishing diffraction peaks at 38.4°, 44.5°, and 64.8° were observed in Au-μPADs (curve b), which matched well with the (111), (200) and (220) crystallographic planes of cubic respectively (JCPDS card No 004-0784).

As can be seen in Figure 2A and 2B, the synthesized Au NPs with uniform shape and size were examined by TEM, which indicated that an almost spherical morphology with a diameter about 15 nm (inset figure) was obtained. The EDX mapping of CeO_2 which included Ce, O element peaks, demonstrating its successful synthesis as depicted in Figure 2C. Furthermore, the SEM images can be seen in Figure 2D, it shows that obtained CeO_2 exhibited a spherical-like shape. The inset figure showed the size distribution of CeO_2. The size of CeO_2 was about 50 nm, which was agreed with the size of SEM showed. In addition, similar results were obtained by the corresponding TEM characterization in Figure 2E. Finally, XRD patterns of the products (Figure 2F) clearly show that all of the peaks appear at 2θ =28.5°, 33.0°, 47.4°, and 56.3°can be indexed from (111), (200), (220), and (311) reflections (JCPDS No. 34-0394) of fluorite-phase CeO_2.

3.3. Electrochemical characterization of the proposed biosensor

The cyclic voltammograms (CV) technique was utilized to characterize the electrode interface in the assembly process of sensing as shown in Figure 3A. Clearly, a well-defined redox peak of $[Fe(CN)_6]^{3-/4-}$ was appeared in the bare μPADs (curve a). When the Au NRs were modified on the paper electrode, the electrochemical signal (curve b) being amplified due to the excellent conductivity of Au NRs, proving that Au NRs could accelerate the electron transfer. A dramatic decrease of peak current

intensity was observed (curve c) after HP was immobilized onto electrode surface, owing to the diffusion of ferricyanide was blocked toward the electrode surface. After blocking with insulating HT, peak current response decreased again (curve d). A significantly weaker current appeared (curve e) followed by the addition of target miRNA owing to the diffusion block of DNA, indicating HP was opened by miRNA. Once S1 labelled probe was introduced onto the prepared electrode, the peak current continuously decreased (curve f) attributed to the increase of steric hindrance, indicating that S1 and capDNA could be complementary. Finally, after conductive $Ru(NH_3)_6^{3+}$ were attached onto the electrode surface, an increasing peak current were observed (curve g), indicating that $Ru(NH_3)_6^{3+}$ could accelerate the electron transfer efficiently. Figure 3B depicted the electrochemical impedance spectroscopy (EIS) Nyquist plot which is a sensitive technique for characterizing electrode surface in the modification process of sensing platform. EIS experiments were performed in the phosphate buffer solution (PBS 0.1 M, pH 8.0) containing 5 mM $[Fe(CN)_6]^{3-/4-}$ and 0.1 M KCl, and the frequency range was at 100 MHz to 10 KHz. In typical impedance spectrum, the semicircle diameter at higher frequencies is related to the electron-transfer resistance (Ret), which dominates the electron transfer kinetics of the redox probe at the electrode interface. Moreover, the linear part at lower frequencies corresponds to the diffusion process of redox probe. A small Ret value of 67.7 Ω for bare μPADs (curve a) was observed. An almost straight line was obtained on the surface of Au-μPADs electrode (curve b), which might be attributed to excellent electrical conductivity of Au NRs to reduce resistance of the electron-transfer. However, the Ret value was increased to 281 Ω and 475 Ω with the stepwise modification of HP and HT (curve c and d) respectively due to the assembled biological molecule blocking the diffusion of ferricyanide toward the electrode surface. Subsequently, target miRNA was hybridized with HP, and remarkable increase of Ret to 566 Ω was observed (curve e) owing to the electrostatic repulsion between miRNA phosphate backbone and the $[Fe(CN)_6]^{3-/4-}$ ions. Finally, after electrochemical probe was successive assembled on electrode by hybridization between HP and capDNA, a gradually increased Ret were observed in curve f,

attributed to the increase of steric hindrance. However, the Ret value significantly decreased to 310 Ω as shown in curve g, which could be attributed to improvement of electrostatic interaction between $[Fe(CN)_6]^{3-/4-}$ and positively charged metal ion. It was found that these results obtained from the EIS were consistent with that in CV, indicating the successful fabrication of miRNA sensing platform.

In this work, to test the advantages of proposed protocol, current responses of the sensing platform incubated with different labelled probe were investigated in the same concentration of target miRNA (1.0 nM) as shown in Figure 3C. It was clear to observe peak current of the biosensor incubated with spherical-like CeO_2 was -9.35 μA (curve a), indicating that CeO_2 possessed catalytic performance toward TMB by H_2O_2. Moreover, the peak current was remarkably enhanced to -15.40 μA when the sensing platform incubated with CeO_2 and Au@GOx as shown in curve b. This phenomenon was ascribed to more efficient catalytic effect produced in the presence of Au NPs, which play the important role in the signal amplification for detection of miRNA. Furthermore, in the presence of $Ru(NH_3)_6^{3+}$, the peak current is higher than that in the absence of $Ru(NH_3)_6^{3+}$ as we predicted in curve c, indicating that the interposition of $Ru(NH_3)_6^{3+}$ molecules to DNA duplex by electrostatic attracting leading to great enhancement of electron transfer efficiency and improve detection sensitivity of proposed assay. In the proposed protocol, GOx plays an important role in catalyzing glucose to generate H_2O_2. In order to ensure the successful loading of GOx to the Au NPs surface, the comparison of the performances of the assay with or without GOx is shown in Figure 3D. Almost no current is generated in curve a compared to curve b, which could be attributed to the fact that generation of H_2O_2 could not accompanied in the absence of GOx leading to the failure of reduction. Therefore, the comparison results displayed that spherical-like CeO_2, Au NPs, $Ru(NH_3)_6^{3+}$ and GOx could enormously enhance the current response, so it plays an crucial role for enhancement of detection sensitivity.

Figure 3

3.4. Performance of the miRNA biosensor

In order to improve the sensitivity of sensing platform, the quantitative behavior of the proposed biosensor was researched on electrochemical response under the optimization of experimental conditions (Figure S5). As depicted in Figure 4A, the electrochemical signal intensity gradually increased with increasing concentration of miR-21 in range of 1.0 fM to 1000 fM, indicating that more electroactive material fixed on the electrode surface. As a result, an excellent linear relationship between the current intensity and the logarithm of miR-21 concentrations can be observed. The corresponding linear regression equation of the calibration curve could be represented as $I = -2.55 - 6.22 \lg C_{miRNA}$ with a correlation coefficient of 0.9966. The detection limit for miR-21 was 0.434 fM which was estimated at a signal-to-noise ratio of 3. The detection limit and linear range of the proposed biosensor were comparable or better than other previous reports with different detection methods listed in Table S2, demonstrating that the proposed biosensor has high sensitivity for detection of miR-21. In order to detect miRNA more simply and quickly, the semi-quantitative were performed in 0.1 M PBS (pH 8.0) containing 6 mM of glucose and 0.8 mM of TMB and 10 U of Exo I with varying concentrations of miRNA as displayed in Figure 4B. The linear equation was $Y=30.94+18.99 \lg C_{miRNA}$ with correlation coefficient of 0.9969, where Y was the grey intensity. The color intensity was proportional to the logarithm concentration of miRNA with the linear range of 10 fM to 1000 fM. The limit of detection was 7.382 fM which was estimated at a signal-to-noise ratio of 3. Moreover, the steady-state kinetic study is presented in the supplementary information. The color changes of TMB can be read out directly by naked eye without complicated instruments. We can conclude that the increasingly dark blue could be observed with the increasing of miR-21 concentration.

3.5. Stability, reproducibility, and selectivity of the biosensor

The stability which is a key factor for proposed biosensor was assessed via testing the electrochemical responses change of the sensing electrode. Five as-prepared sensing paper electrodes were first fabricated in the same conditions and stored at different times (0, 5, 15, 25 and 30 days) at 4℃. As can be seen in Figure 4C,

a 92.7% decrease of initial response was found within 30 days, implying the biosensor had satisfying storage stability. To evaluate the reproducibility of the proposed platform, the batch-to-batch precision and the same batches was studied toward the same concentration of miR-21 (1 pM). Similar electrochemical signals and relative standard deviation (RSD) of 3.2% for the same batch biosensor with five parallel determinations and RSD of 4.4% for different batch biosensor with five biosensors were obtained. These results demonstrated that the reproducibility of the proposed method was acceptable.

The selectivity of proposed platform was investigated by comparing the electrochemical signals of the possible interferences, including one-base mismatched RNA (sRNA), miR-210, and miR-155. As exhibited in Figure 4D, similar electrochemical signals and relative standard deviation (RSD) of 2.1%, 2.6%, 1.3%, 1.6%, 1.4%, and 1.1% were obtained in the measurement of mix, miR-21, miR-155, miR-210, sRNA and blank. Therefore, a negligible electrochemical response to sRNA, miR-210, and miR-155 (10 pM) were observed when the biosensor was incubated with miR-21 (1 pM). Additionally, the current responses of miR-21 displayed an obvious increase than that of the blank solution. In addition, the electrochemical intensity of the mixture containing the above three interferents in the presence of miR-21 was almost identical to those without interference. Therefore, this result demonstrated that only the completely matched sequence could trigger signal amplification strategies, indicating that an excellent selectivity was obtained.

3.6. Application in analysis of samples

To investigate the analytical reliability and application potential of the proposed biosensor, the recovery experiments were performed by adding a series of synthetic miR-21 with different concentration into the 10-fold diluted healthy human real serum sample (acquired from Cancer Research Center of Shandong Tumor Hospital, China). The results shown in Table S3, good recoveries from 98.8% to 101.3% and the RSD

values from 1.8 to 3.6 indicated that the prepared platform has potentiality in examination of miR-21 in real clinical analysis.

4. Conclusions

In summary, we have successfully developed a biosensor which achieved signal amplification based on CeO_2-Au@GOx as a signal material to detect target miR-21 by designing a multifunctional μPADs. For the rapid and precise detection of miR-21, the semi-quantitative analysis combined with quantitative analysis was applied to the proposed protocol. The paper-based electrochemical sensing platform was approved to have wide linear range (1.0 fM to 1000 fM), low detection limit (0.434 fM), good stability, excellent reproducibility, high selectivity and satisfying sensitivity for miR-21 detection, which providing a promising platform for point-of-care diagnosis in clinical applications. However, the proposed biosensor cannot achieve simultaneous detection of multi-targets in a paper-based analytical device. For this purpose, we will attempt to find a more convenient method to detect multi-targets on one paper-based analytical device.

Acknowledgment

This work was financially supported by the National Natural Science Foundation of China (21575051, 21775055, 21501090, 21475052), Natural Science Foundation of Shandong Province, China (2017C01-3) and the program for Taishan Scholars.

References

Cheng, F., He, T., Miao, H., Shi, J., Jiang, L., Zhu, J., 2015. ACS Appl. Mater. Interfaces. 7, 2979-2985.

Cissell, K.A., Rahimi, Y., Shrestha, S., Hunt, E.A., Deo, S.K., 2008. Anal. Chem. 80, 2319-2325.

Fang, S., Lee, H.J., Wark, A.W., Corn, R.M., 2006. J. Am. Chem. Soc. 128, 14044-14046.

Ge, S., Lan, F., Lang, L., Ren, N., Li, L., Liu, H., Yan, M., Yu, J., 2017. Acs Appl. Mater. Interfaces. 9, 6670-6678.

Graybill, R.M., Bailey, R.C., 2016. Anal. Chem. 88, 431-450.

Hou, T., Li, W., Liu, X., Li, F., 2015. Anal. Chem. 87, 11368-11374.

Jampaiah, D., Srinivasa Reddy, T., Kandjani, A.E., Selvakannan, P.R., Sabri, Y.M., Coyle, V.E., Shukla, R., Bhargava, S.K., 2016. J. Mater. Chem. B. 4, 3874-3885.

Jiao, X., Song, H., Zhao, H., Bai, W., Zhang, L., Lv, Y., 2012. Anal. Methods. 4, 3261-3267.

Li, Y., Zhang, Y., Li, F., Feng, J., Li, M., Chen, L., Dong, Y., 2017. Biosens. and Bioelectron. 92, 33-39.

Liu, B., Sun, Z., Huang, P.-J.J., Liu, J., 2015. J. Am. Chem. Soc. 137, 1290-1295.

Liu, H.Y., Tian, T., Ji, D.D., Ren, N., Ge, S.G., Yan, M., Yu, J.H., 2016. Biosens. and Bioelectron. 85, 909-914.

Liu, J., Zhang, L., Lei, J., Ju, H., 2015. ACS Appl. Mater. Interfaces. 7, 19016-19023.

Liu, S., Wang, C., Zhang, C., Wang, C., Wang, Y., Tang, B., 2013. Anal. Chem. 85, 2282−2288.

Ma, F., Liu, M., Tang, B., Zhang, C., 2017. Anal. Chem. 89, 6182−6187.

Mahmoud, A., Mojtaba, S., Reza, S., Saeed,S., Vahid E., 2017. Biosens. and Bioelectron. 98, 113-118.

Martinez, A.W., Phillips, S.T., Butte, M.J., Whitesides, G.M., 2007. Angew. Chem. 46, 1318-1320.

Martinez, A.W., Phillips, S.T., Whitesides, G.M., Carrilho, E., 2010. Anal. Chem. 82, 3-10.

Mitsudome, T., Yamamoto, M., Maeno, Z., Mizugaki, T., Jitsukawa, K., Kaneda, K., 2015. J. Am. Chem. Soc. 137, 13452-13455.

Shao, Q., Wu, P., Gu, P., Xu, X., Zhang, H., Cai, C., 2011. J. Phy. Chem. B. 115, 8627-8637.

Su, S., Nutiu, R., Filipe, C.D.M., Li, Y., Pelton, R., 2007. Langmuir. 23, 1300-1302.

Tao, Y., Yin, D., Jin, M., Fang, J., Dai, T., Li, Y., Li, Y., Pu, Q., Xie, G., 2017. Biosens. and Bioelectron. 96, 99-105.

Thomson, J.M., Parker, J., Perou, C.M., Hammond, S.M., 2004. Nat Methods. 1, 47-53.

Torrente-Rodríguez, R.M., Campuzano, S., Montiel, V.R.-V., Montoya, J.J., Pingarrón, J.M., 2016. Biosens. and Bioelectron. 86, 516-521.

Wei, Y., Li, Y., Li, N., Zhang, Y., Yan, T., Ma, H., Wei, Q., 2016. Biosens. and Bioelectron. 79, 482-487.

Yan, P., Wang, R., Zhao, N., Zhao, H., Chen, D.-F., Xu, F.-J., 2015. Nanoscale. 7, 5281-5291.

Yang, H., Zhang, Y., Li, L., Zhang, L., Lan, F., Yu, J., 2017. Anal. Chem. 89, 7511-7519.

Ye, S., Li, X., Wang, M., Tang, B.,2017. Anal. Chem. 89, 5124−5130.

Zhang, L., Zhang, S., Pan, W., Liang, Q., Song, X., 2016. Biosens. and Bioelectron. 77, 144-148.

Figure Captions

Scheme 1 Schematic illustration of the stepwise miRNA biosensor fabrication process

Scheme 2 (A) The schematic representation, size, and shape of μPADs. (B) The fabrication of microfluidic paper-based analytical devices for detection of miRNA combining chromogenic reaction and electrochemistry.

Figure 1 SEM images of (A) bare paper, (B) as-prepared Au NRs modified paper, (C) under further magnifications, (D) XRD image of bare paper (a), and Au NRs modified paper (b).

Figure 2 Typical TEM images of (A) the prepared Au NPs, (B) under further magnifications, inset: the dynamic light scattering size-distribution of Au NPs; (C) EDX image, (D) SEM image, (E) TEM image, (F) XRD pattern of spherical-like CeO_2, inset: the dynamic light scattering size-distribution of CeO_2.

Figure 3 CVs (A) and EIS (B) for each immobilized step in 5 mM $[Fe(CN)_6]^{3-/4-}$ solution containing 0.1 M KCl: (a) bare μPADs, (b) Au NRs modified μPADs, (c) step

b assembled HP, (d) step c blocked with HT, (e) step d incubated with the miRNA, (f) step e hybridized with electrochemical probe, (g) step f in the presence of $Ru(NH_3)_6^{3+}$. (C) DPV responses of the miRNA biosensor according to different signal amplification strategies: (a) catalysis of CeO_2, (b) modified with CeO_2-Au@GOx, (c) interposition of $Ru(NH_3)_6^{3+}$. (D) DPV responses of the miRNA biosensor in the absence (a) or presence (b) of GOx. Curve a in (C) was detected in 0.1 M PBS containing 2 $mg \cdot mL^{-1}$ GOx and 6mM glucose, while the other detection were performed in 0.1 M PBS containing 6 mM glucose.

Figure 4 (A) The calibration plots of DPV peak current vs the logarithm of miR-21 concentration; insert: DPV responses of the proposed biosensor with different miR-21 concentrations in 1 mL of 0.1 M PBS (pH 8.0) containing 6 mM of glucose: (a) 0 fM, (b) 1 fM (c) 5 fM, (d) 10 fM, (e) 50 fM, (f) 100 fM, (g) 500 fM, (h) 1000 fM. (B) The calibration plots of color intensity vs the logarithm of miR-21 concentration; insert: Photographs of biosensor based on chromogenic reaction in the different amounts of miRNA. From left to right: the concentration of miR-21 is 0, 10, 20, 50, 100, 500, 1000 fM, respectively. (C) The storage stability of the miRNA biosensor in a refrigerator (4℃). (D) Selectivity investigation of the biosensor (blank sample, 10 pM sRNA, 10 pM miR-210, 10 pM miR-155, 1 pM miR-21, mixture of forenamed miRNA with the same concentration of 1 pM).

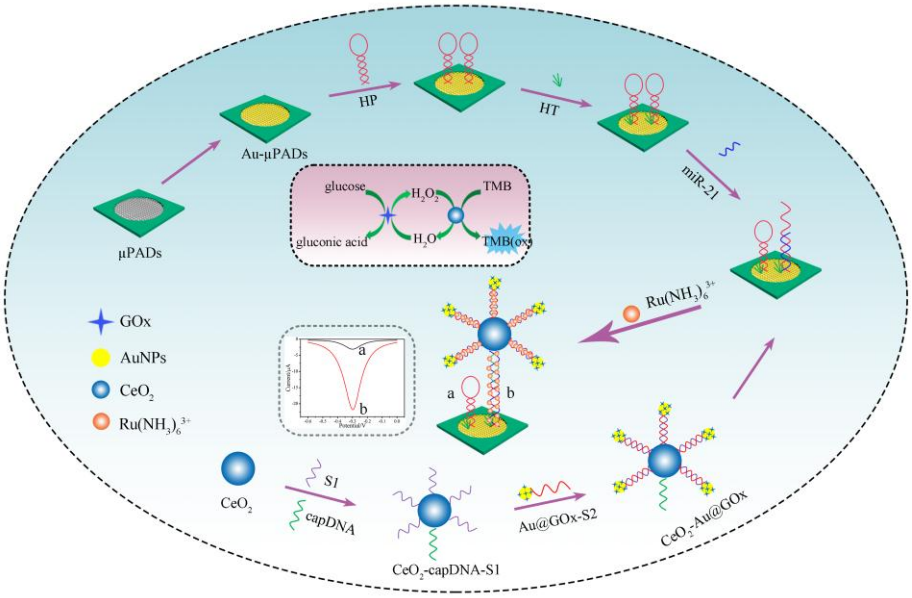

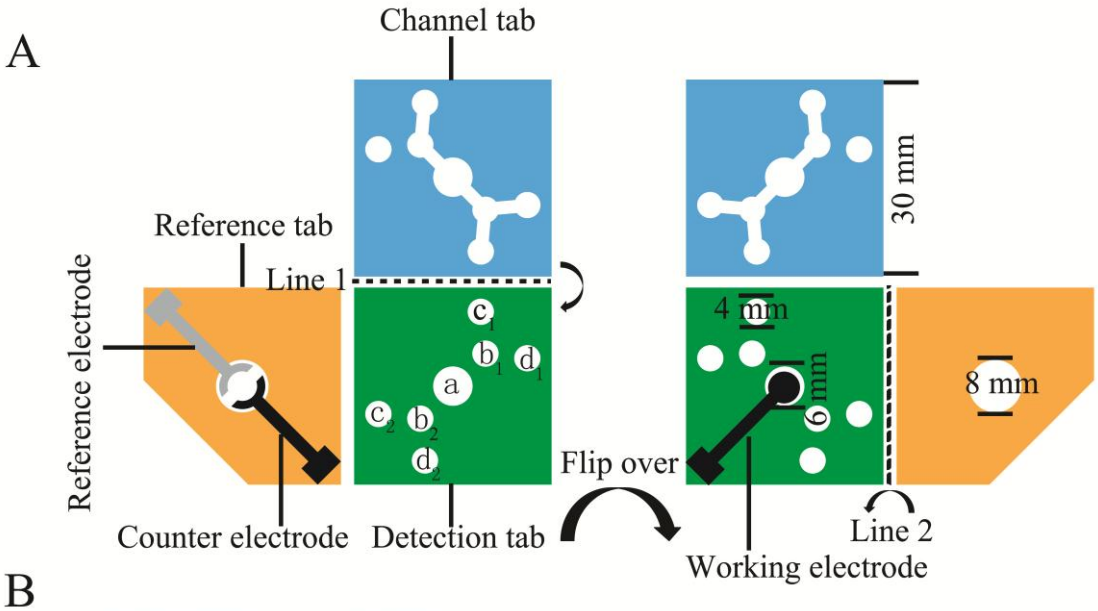

B

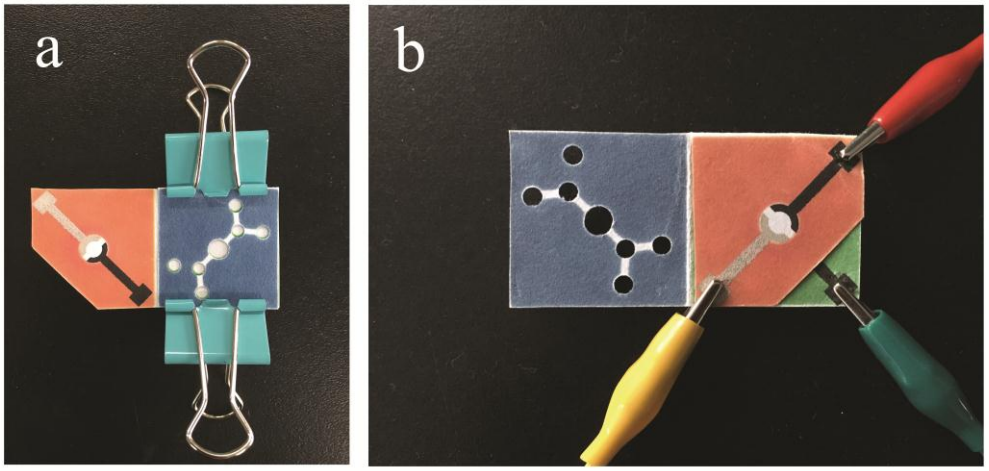

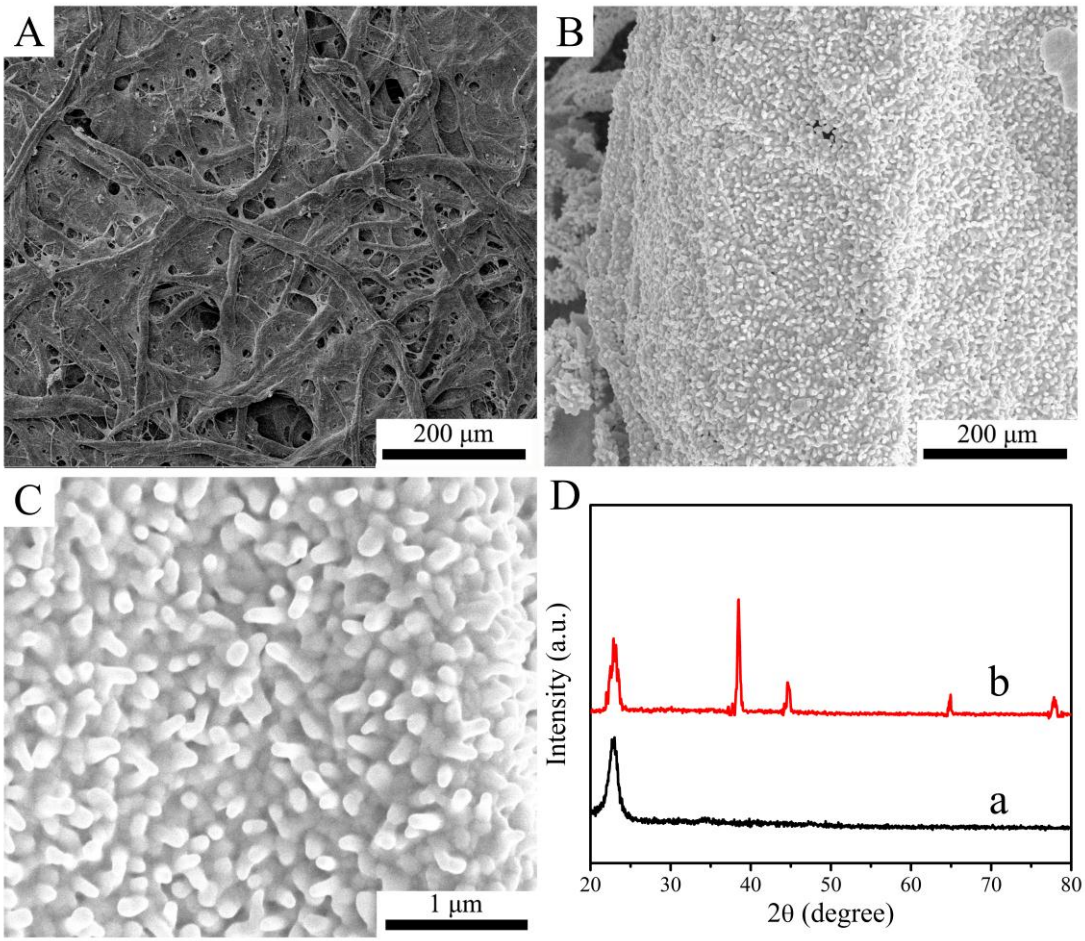
A
200 μm
B
200 μm
C
1 μm
D
Intensity (a.u.)
b
a
20
30
40
50
60
70
80
2θ (degree)

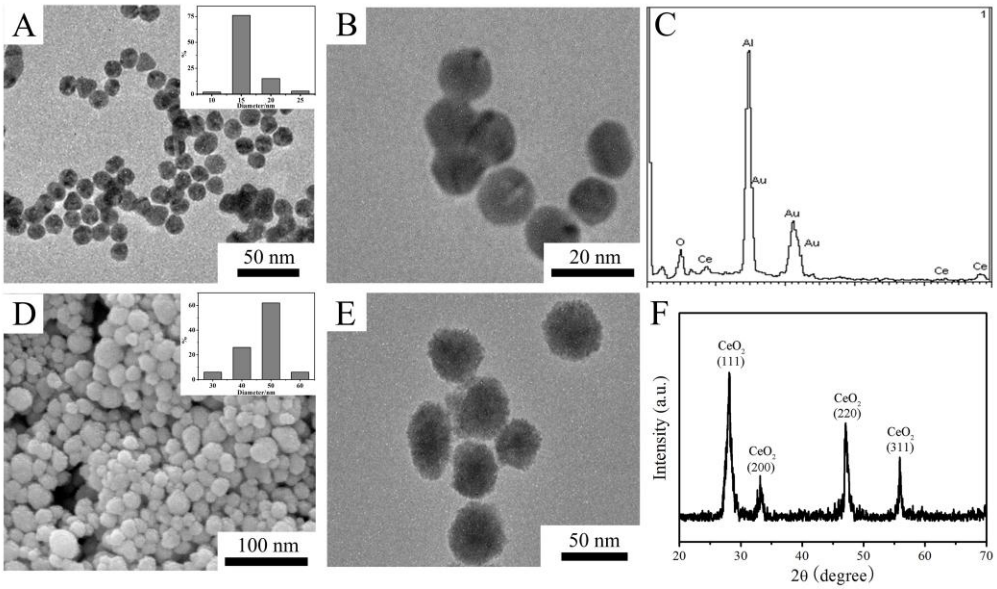
A
50 nm
B
20 nm
C
Al
Au
Au
Au
O
Ce
Ce
Ce
D
100 nm
E
50 nm
F
Intensity (a.u.)
CeO2 (111)
CeO2 (200)
CeO2 (220)
CeO2 (311)
20
30
40
50
60
70
2θ (degree)

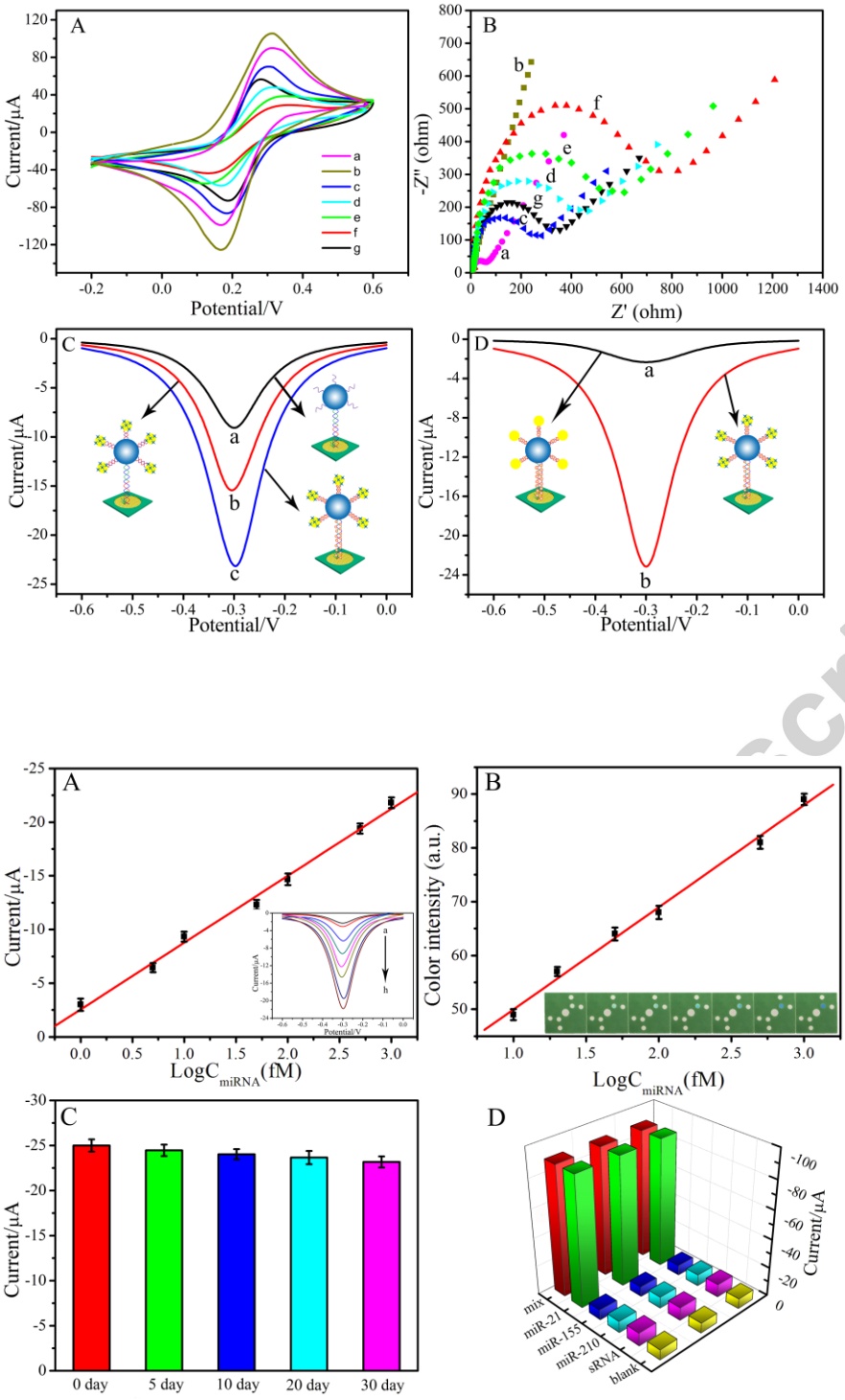

Highlights

- Spherical-like cerium dioxide was synthesized for catalysis.
- DNA functionalized composite as an electrochemical probe was applied for amplification strategy.

- Microfluidic paper-based analytical devices provide an interesting method for semi-quantitative detection and quantitative detection.
- Microfluidic paper-based electrochemical/visual biosensor was developed for miR-21 detection.